Ground-penetrating radar as a tool for probing the shallow subsurface of Mars

John A. Grant

Center for Earth and Planetary Studies, National Air and Space Museum, Smithsonian Institution, Washington, D. C., USA

Alan E. Schutz

Geophysical Survey Systems, Inc., North Salem, New Hampshire, USA

Bruce A. Campbell

Center for Earth and Planetary Studies, National Air and Space Museum, Smithsonian Institution, Washington, D. C., USA

[1] Design and testing of an impulse ground-penetrating radar (GPR) for possible rover deployment on Mars in 2009 is well underway. The GPR has mass, power, volume, and data-rate targets of 0.5 kg, 3 W (peak), 3400 cm^3, and 0.3 Mb/d and will possess easily modified bistatic high-frequency (e.g., 500–600 MHz) and monostatic "rat-tail" (e.g., 100 MHz) antennas. The GPR should be capable of measuring in situ radar properties on Mars to depths of up to 10–20 m, thereby helping to constrain near-surface geology and structure. Initial GPR tests at the site of the 2001 FIDO rover field trials near Cronese Lake, California, confirm the value of the instrument in defining local geologic setting and in providing context for data collected using other rover science payload elements. A rover-deployed GPR may enable three-dimensional mapping of local stratigraphy, which in turn can assist in evaluating the history of aqueous activity and the accessibility of near-surface water. *INDEX TERMS:* 0994 Exploration Geophysics: Instruments and techniques; 0933 Exploration Geophysics: Remote sensing; 5494 Planetology: Solid Surface Planets: Instruments and techniques; 5464 Planetology: Solid Surface Planets: Remote sensing; 5460 Planetology: Solid Surface Planets: Physical properties of materials; *KEYWORDS:* Radar, Mars, water, rover, geophysics, stratigraphy

1. Introduction

[2] Radar is a fundamental tool that is capable of addressing a variety of geological problems on the Earth and other planets. Terrestrial radar applications over the past 30 years have increased dramatically and include orbital imaging systems [e.g., *Elachi*, 1986], airborne imaging systems [e.g., *Evans et al.*, 1986], and surface-based ground-penetrating systems [e.g., *Ulriksen*, 1982]. Airborne and orbital imaging radar data are most often used to characterize surface roughness and reflectivity, particularly at frequencies in the X- and C-band ranges (3–6 cm wavelength) [e.g., *Arvidson et al.*, 1992; *Gaddis*, 1992; *Campbell et al.*, 1993; *Campbell and Shepard*, 1996]. At L- and P-band frequencies (24–70 cm wavelength), both surface and volume scattering effects are observed. Significant volume scattering is generally associated with smooth-surfaced deposits of fine-grained or very dry material [*Schaber et al.*, 1986].

[3] A ground-penetrating radar (GPR) operates by placing a monostatic (single-element for transmit and receive) or bistatic (independent transmit and receive elements) antenna in close proximity to a surface of interest. One mode of operation involves a pulse generator that applies a narrow pulse of energy to the antenna, which acts as a band-pass filter, and produces a single sine wave cycle that is broadcast. The returned echoes are then collected as a function of time. An alternate mode of operation uses a step-frequency or "chirp" technique to form radar pulses. This method utilizes a spread in frequency to permit synthesis of a short effective pulse from a much longer transmitted signal. The planetary GPR discussed here uses a more simple impulse generator, for which the pulse width and the propagation velocity in the target medium are used in setting the range resolution.

[4] GPR data provide "ground truth" for measurements collected by imaging and sounding radar systems. In planetary radar remote sensing, the emphasis is often on characterizing volume scattering from regoliths and mantling layers [*Thompson et al.*, 1970; *Campbell et al.*, 1997]. Mars has been shown to have a wide range of radar scattering properties in the wavelength range from 3 to

13 cm, with evidence for extensive volume penetration, scattering from buried terrain, and variations in electric or magnetic loss properties [*Muhleman et al.*, 1991; *Simpson et al.*, 1992; *Butler et al.*, 1993; *Butler*, 1995; *Muhleman*, 1995; *Harmon et al.*, 1999]. Orbital sounding radars can provide a view from 100's of meters to several km in-depth [*Phillips et al.*, 1973; *Peeples et al.*, 1978]. Interpretation of imaging/sounding radar data is non-unique, however, as the physical and dielectric properties of the near-surface environment are often poorly known. GPR data can be used to characterize near-surface geology, structure, and may define dielectric properties, thereby allowing extrapolation of local information to the regional scale offered by orbital sensors [*Olhoeft and Strangeway*, 1974; *Barbin et al.*, 1995; *Grant et al.*, 1995a; *Ori and Ogliani*, 1996; *Grant and Schutz*, 1998; *Olhoeft*, 1998a].

[5]   While GPR has not yet been deployed on the surface of Mars, it has been proposed for a previous Russian mission [*Institute for Space Research*, 1992; *Barbin et al.* 1995], a future French mission [*Reineix et al.*, 2001], and a future U.S. mission [*Grant and Schultz*, 1992; *Paige*, 1994; *Planetary Surface Instrument Workshop*, 1995; *Grant and Schutz*, 1998; *Olhoeft*, 1998a; *Plaut*, 1998; *Grant et al.*, 2001; *Beaty et al.*, 2001; *Clifford et al.*, 2001].

[6]   We first discuss the scientific rationale for considering a rover-deployed Mars GPR. An overview of environmental factors influencing GPR performance on the Earth and Mars is followed by a description of probable rover limitations on design, and a discussion of our impulse GPR. Next, likely operational scenarios on Mars are described. Finally, we present results of testing at the 2001 FIDO rover field site.

2.   GPR and Mars Science

[7]   The Martian surface records a long and often complex history of geologic activity. Results of geologic mapping [e.g., *Greeley and Guest*, 1987] and new data from the Mars Global Surveyor spacecraft [e.g., *Malin et al.*, 1998; *Malin and Edgett*, 2000, 2001] reveal numerous layered substrates that are often mantled by eolian deposits. While a proposed orbital radar system [*Campbell et al.*, 2001] may probe beneath this mantling layer to reveal subsurface geomorphology, successful rover drilling or other subsurface studies require more detailed information on local stratigraphy and structure. The ability to rapidly and non-intrusively delineate stratigraphy and structure to depths of 10's of meters [e.g., *Grant et al.*, 1997, 1998, 2001; *Olhoeft*, 1998a] highlights the potential utility of an impulse GPR as a tool for constraining geologic setting and providing context for other lander and/or rover instruments on Mars.

[8]   GPR data may not detect water unambiguously on Mars, particularly if near-surface occurrences are in the form of permafrost. Occurrence of liquid water, however, will likely lead to large, easily detected dielectric contrasts. Moreover, definition of stratigraphy and setting will help in evaluating the history of aqueous activity and where any water might occur and be accessible. GPR data can also be used to infer the degree of any post-depositional pedogenic alteration or weathering, thereby enabling assessment of pristine versus secondary morphology.

[9]   A GPR on Mars may assist in penetrating beneath a mantle of eolian drift [*Christensen*, 1986; *Malin et al.*,

1998; *Malin and Edgett*, 2001], help define the character of northern lowland stratigraphy to distinguish an alluvial versus volcanic [e.g., *Greeley and Guest*, 1987; *Golombek et al.*, 1997] versus pelagic origin [*Parker et al.*, 1989; *Head et al.*, 1999; *Thomson and Head*, 2001], and could constrain the origin of the "Stealth" and other radar-defined units [*Goldstein and Gillmore*, 1963; *Dyce et al.*, 1967; *Muhleman et al.*, 1991; *Muhleman*, 1995; *Butler*, 1995]. In situ discrimination of any carbonates [*Fanale et al.*, 1982; *Blaney and McCord*, 1990], sulfates [*Toulmin et al.*, 1977; *Settle*, 1979], or near-surface brines/salts [*Zent et al.*, 1990], might also be accomplished. Finally, possible evidence for life on Mars [*McKay et al.*, 1996] leads to questions of where and when such life may have occurred. An obvious place for in situ investigation of past biological activity would be in depositional sinks [e.g., *Goldspiel and Squyres*, 1991; *Goldspiel et al.*, 1993; *Grant*, 2000]. A rover-deployed GPR could help delineate stratigraphy in these sinks and pinpoint sediments that may have harbored past life.

3.   Design of a Rover-Deployable GPR for Mars

[10]   In recognition of the potential for constraining near-surface stratigraphy and structure on Mars, development of a miniaturized impulse GPR is well underway. Efforts are focused on design and testing of prototype antennas in parallel with fabrication of a control unit with low power, mass, and volume requirements that consolidates all function and extended memory onto a single board. Antenna development emphasizes a design that is easily adaptable to rover deployment on a range of planetary surfaces. As such, the capabilities of the antennas cover a range of expected surface properties and can be focused on maximizing performance in a specific geologic setting. The operational depth of 10–20 m is geared toward defining stratigraphy, subsurface cobble or block distribution, and structure at the decimeter-to-meter scale. This target operational depth avoids the need for a higher power, swept- or step-frequency radar system geared toward deeper penetration.

3.1.   Factors Affecting GPR Performance

[11]   Ground-penetrating radar has evolved as an important tool for probing the shallow subsurface in a variety of geologic settings when deployed from surface, underwater, and airborne platforms [e.g., *Ulriksen*, 1982; *Olhoeft*, 1988, 1998b; *Grant et al.*, 1995a, 1995b, 1998]. An impulse GPR uses an emitted bipolar radar wave to delineate subsurface interfaces between materials with contrasting dielectric, magnetic, and/or structural or geometric properties [e.g., *Olhoeft*, 1998a]. The complex dielectric properties (which include electric permittivity, magnetic permeability, and conductivity) and geometry of potential scattering/reflecting layers or objects must all be considered when designing a planetary GPR.

[12]   The real dielectric constant of most natural materials is determined largely by moisture content, grain size, clay content, and porosity, and for dry materials ranges between 2 and 15 [*Ulriksen*, 1982; *Ulaby et al.*, 1988]. The presence of water with dissolved salts can rapidly raise the real dielectric constant to values approaching ∼80. In Mars applications, the target surface is expected to be dry or

Table 1. Range in Value for Radar Loss Tangent Inferred for the Martian Near Surface

Value	Material	Notes	Reference
0.004 – 0.03	basalt, ash, carbonate sediments	Terrestrial values not correlated with specific materials/compositions	*Biccari et al.* [2001]
No values ~10 times λ[a]	Analogy with lunar materials	Assumed to relate to basaltic and or anorthositic compositions	*Simpson et al.* [1992]
0.05 – 0.3	Laboratory analogs	Variety of Materials	*Heggy et al.* [2001]
0.01	Average Surface	Assumes very dry substrates	*Plaut* [1998]
0.0255 – –0.25	Unknown	Model used for Netlander	*Reineix et al.* [2001]

[a]λ, radar wavelength.

frozen, so liquid water effects on the dielectric constant will be minimal. The dielectric loss factor ranges over several orders of magnitude with mineralogy (e.g., iron or titanium abundance), but has little correlation with sample density [*Ulaby et al.*, 1988].

[13] The magnetic properties of natural materials are less well understood, but occurrence of appreciable iron-bearing minerals can lead to significant magnetic losses [*Olhoeft*, 1998a, 1998b]. Magnetic losses can exceed electrical losses where iron-bearing minerals account for greater than 20–30% of a substrate by weight [*Olhoeft*, 1998a], and these losses are largely insensitive to operating frequency (in the range of 50 MHz to 1 GHz [see *Olhoeft*, 1998a]) for a constant temperature. A paucity of experimental data on the role of magnetic losses warrants further research into their effects.

[14] The geometry of potential scattering layers and objects also has a significant impact on the utility of a GPR. Scatterers or reflectors at greater distances from the sensor have lower radar returns due to spreading of the incident energy and increasing attenuation with path length. Scattering effects become significant when objects are present (cobbles, blocks, fractures, etc.) whose size is greater than ~1/3–1/2 the radar wavelength [*Olhoeft*, 1998b]. The effective reflectivity of any layer interface or scatterer is a function of its dielectric contrast with the neighboring material.

[15] Careful consideration of these factors leads to confidence that a rover-deployed GPR on Mars can achieve 10–20 m penetration. Low ambient temperature and/or dry conditions in the near surface should reduce electrical losses. These dry conditions should help to mitigate difficulties related to the possible presence of abundant fine-grained material or salts in some locales [*Collins and Kurtz*, 1998; *Malin et al.*, 1998]. Although dielectric values of 3–10 and dry conditions likely characterize the near-surface of Mars [*Simpson et al.*, 1992; *Muhleman*, 1995; *Barbin et al.*, 1995; *Plaut*, 1998], corresponding loss tangents remain incompletely understood [*Leuschen et al.*, 2001], but may be as high as ~0.3 (Table 1) [*Heggy et al.*, 2001]. Such high losses might limit deep radar penetration, but would permit penetration depths on the order of 10 times the radar wavelength [*Simpson et al.*, 1992]. For systems operating in the range of 100–600 MHz, penetration to depths of up to 10–20 m should be possible.

[16] Magnetic losses are likely to be important only in substrates with significant iron-bearing minerals. While recent studies suggest iron-bearing materials may be abundant in some places on Mars [*Banin et al.*, 1992; *Rieder et al.*, 1997; *Acuna et al.*, 1999], careful landing site selection can help in avoiding highly lossy terrains. Radar signal clutter will occur from reflections off the rover and as a result of internal clutter in the antennas and electronics. Because the clutter will be stationary, however, it can be removed via subtraction from the data during post-processing. Finally, geometric factors related to spreading can be mitigated to some degree by maximizing power transmitted into the ground and/or averaging multiple scan lines to increase signal-to-noise ratios. A strength of our generic antenna design is that the frequency can be easily modified to improve operation in various target substrates.

3.2. Platform Constraints on a Mars GPR

[17] A critical factor in optimizing the effectiveness of a rover-deployed GPR involves limits on mass, power, volume, and deployment configurations imposed by rover interfaces and operational requirements. We have adopted the general design of the rovers flown or being tested for the Mars Exploration Program (e.g., Sojourner, and the Mars Exploration Rovers) as a means of defining these constraints (Figure 1). These designs suggest that future Mars rovers will likely be at least ~40–50 cm wide, ~65–75 cm long, and ~30–45 cm high. Moreover, ground clearance should be at least ~15 to 20 cm, and the rover wheelbase will extend slightly beyond the body with dimensions of ~60 cm wide by ~105 cm long.

[18] Likely interface requirements indicate mass, power, and volume limits of 0.5 kg, 3 W (peak), and 3400 cc, respectively. Similarly, the realities of returning data from the surface of Mars require that the system possess a fairly low data rate. The need to ensure that deployment of the GPR antennas does not interfere with rover mobility and operations dictates a strong desire to keep them elevated above the surface where an ability to easily deploy and retract adds flexibility in data collection. Because many rover components (including the wheels) will be metallic, and because electrostatic charging by dust may be important, the GPR will need to be in a sealed metal box that is grounded to the rover frame. More significant design modifications required by electrostatic charging are unlikely: the above ground deployment of the bistatic antenna precludes the need for isolation from the rover and any unexpected problems associated with the low-frequency component could ultimately be mitigated by utilizing the rover as part of the antenna.

3.3. GPR System Design

[19] Our focus is on design of a simple impulse GPR system with the flexibility to define geologic characteristics in a variety of potential target media. Assembly of the breadboard GPR is derived from existing commercial designs and methods employed at Geophysical Survey
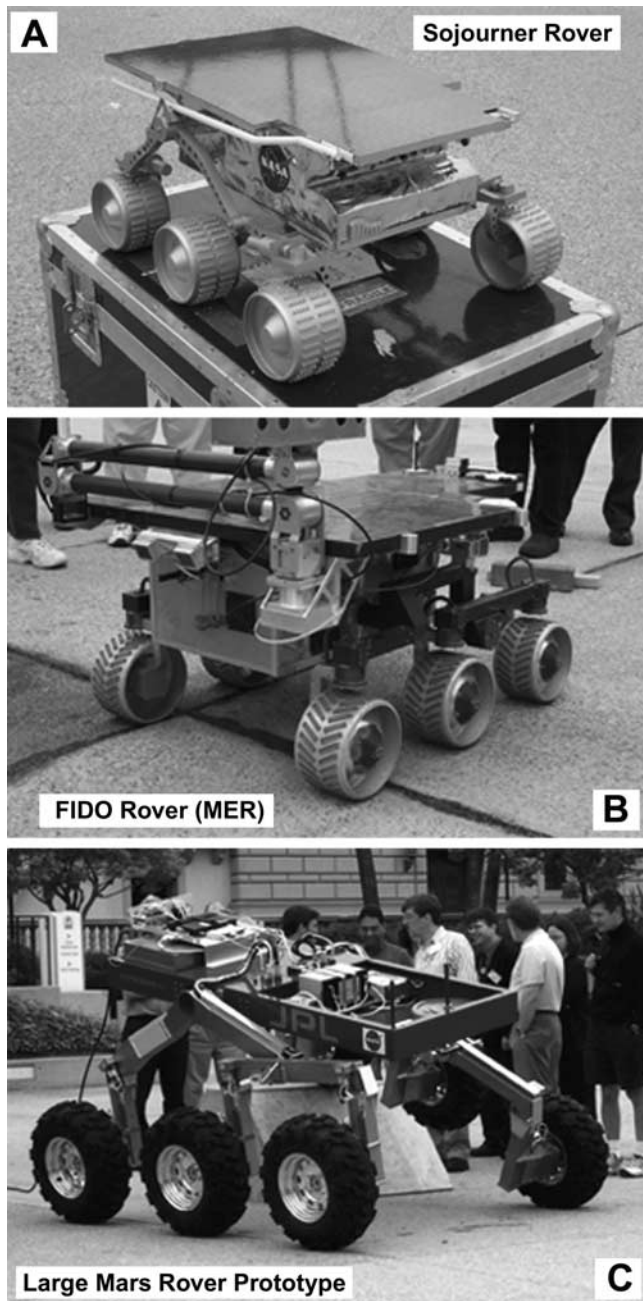
Figure 1. Engineering models of rovers having flown or under development for possible future flight to Mars. Rovers demonstrate the range in possible platform characteristics that must be considered in development of a rover-deployable GPR and include the (a) Sojourner, (b) FIDO field prototype for the 2003 Mars Exploration Rovers, and (c) a prototype large rover.

Systems, Inc. (GSSI). The prototype GPR system has two antennas with center frequencies of 100 and 600 MHz. Both monostatic and bistatic designs are being considered for the lower-frequency antenna, whereas the higher frequency is bistatic. Both frequencies can be modified without changes to the driving electronics. The maximum probing range is set by the range window, which receives echoes up to 1000 ns after transmission (Table 2). Expected peak power

requirement for operation of the radar is 3 W (including antenna deployment/retraction) with <1 mW standby power, and <10 μW during sleep mode. Average power usage is dependent to a large degree on the data cycle, which is expected to take on the order of 2 seconds (not including deployment). As an extreme example, if GPR deployment and data collection took place every 30 minutes, average power use would be only 3 mW.

[20] A basic block diagram of the GPR system is shown in Figure 2. Design innovations include consolidation of all processor functions and extended memory onto a single board, permitting a major stride toward achieving the stated mass, volume, and power targets. The Digital Signal Processor (DSP) controls all functions, whereas the trigger generator sends pulses to the transmitter that forms the outgoing pulse for the antennas. The received signal is sampled with a very high-speed sample-hold to produce an audio-frequency signal, which is then fed to a high-resolution analog-to-digital (A/D) converter. These digital "words" are sent to the DSP for further processing. A separate communications circuit interfaces with the central processor in the rover.

[21] One of the most critical GPR circuits is the trigger generator (Figure 2), which creates precisely timed pulses for input to the antenna circuits. At present, we are incorporating a trigger generator with 5 ps jitter that can automatically calibrate the circuit before each scan acquisition. The 5 ps jitter is well within the 50 ps requirement cited in Table 2. Consolidation of hardware functions into DSP's lowers the parts count, system size, weight and power, and increases reliability. In addition, use of a DSP with a very large internal RAM eliminates the need for an external RAM cache. Finally, circuitry is being further simplified by use of an efficient, fast responding, power

Table 2. Expected GPR Performance Parameters

|	(High-/Low-Frequency Antennas)
Frequency	600/100 MHz
Receiver Bandwidth	800/400 MHz minimum
Settling time of rf amplifier	200/1000 ps
Sampling noise level	~75°K (0−1 GHz BW)
Linearity	5−10% except for transmit pulse area
Dynamic range	>70 dB
Transmitter Pulse shape	Triangle-shaped, risetime 500/2000 ps, fall-time 5/30 ns. Peak amplitude 50 to 100 volts.
Ring down	Amplitude of transmitted pulse 20 dB down in 4/20 ns
Radiated Peak Power	<3 W
Radiated Average Power	<1 mW
Radiated Average Power per MHz	<1 microwatt/MHz over 50 KHz to 1 GHz
T/R switch Dead band (low-frequency antenna)	20 ns
Max allowable trigger generator jitter	50 ps rms
Sampling time resolution	100 ps
Time base linearity	80 ps peak
Zero time base stability	500 ps
Adjustable Range	10−1000 ns
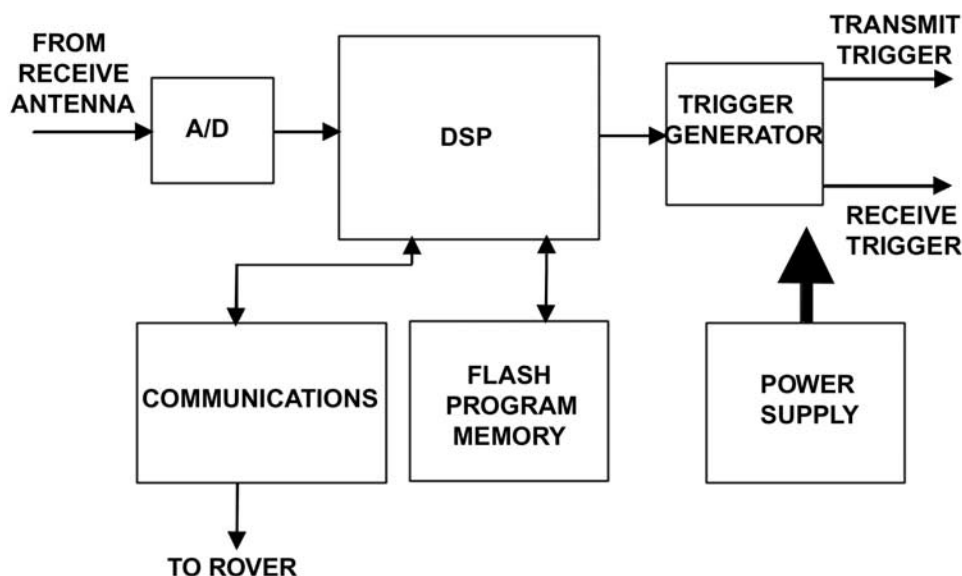
Figure 2. Idealized block diagram of major instrument components associated with development of a miniaturized GPR suitable for possible future rover deployment on Mars. Individual components are discussed in the text. The system currently under design consolidates all control unit function and extended memory onto a single computer board.

supply with low leakage in the off state and that requires a minimal number of different voltages.

3.4. Prototype GPR Antennas for Mars

[22] The GPR will utilize a bistatic high-frequency antenna for high resolution near the surface, and a lower-frequency monostatic (or bistatic) element for deeper sounding. Use of unshielded antennas significantly reduces their size and weight and may be used because there are no overhead clutter targets. Any possible reflections from the rover will be stationary, and may be removed via post-processing of the data. The antenna system can be easily modified by changing the width of the high-frequency antenna fans to increase or decrease the center operating frequency. Both the high- and low-frequency components consist of a very high-speed sample hold circuit that can incorporate an RF amplifier on its front end if desired.

[23] The breadboard high-frequency (600 MHz) antennas are 38-cm-long resistively loaded dipoles mounted on a dielectric rod (Figure 3). Antenna deployment will likely involve a retractable bar with both transmit and receive elements mounted at the outboard end (Figure 3), thereby achieving separation of up to ~70 cm from the back of the rover when fully deployed (assuming operation from a FIDO/MER-class rover, Figure 1b). For initial testing, separation between the transmitting and receiving elements was 25 cm and the antennas were mounted 15 cm above the ground and 30 cm from a metal box that was used as a rover simulator.

[24] Initial testing of the breadboard high-frequency antenna occurred in a test bed of sand overlying first surficial glacial deposits and then deeper, fractured granitic bedrock (Figure 4). Resultant data enables definition of radar reflections to depths exceeding 10 meters (Figure 4) and at a horizontal resolution of tens of centimeters. Bistatic antennas have the advantage of a very short "clear time,"

defined as the period during which the transmitted pulse overlaps any possible subsurface returns. The breadboard system used to drive these antennas operated at a pulse repetition frequency of 64 kHz.

[25] A prototype of the low-frequency (100 MHz) monostatic antenna consisting of a flexible line or "rat-tail" has also been built and successfully tested (Figure 5). Tests with the prototype system confirm the ability to distinguish radar reflections from a dipping surficial deposit-to-bedrock transition from 7 m to up to 15 m depth (Figure 5). As presently designed, the "rat-tail" antenna utilizes a Transmit-Receive (T/R) switch with a switching delay that obliterates the beginning of each scan (to depths of up to ~2–3 meters depending on the dielectric properties of the substrate). To avoid this problem, we have also explored a bistatic mode, with two 40-cm resistively loaded monopoles operating at a central frequency of 100 MHz.

[26] It is anticipated that the low-frequency antenna will either be reeled onto the ground or deployed above the surface using a telescoping or extendable rod (much like an automobile antenna). The above ground deployment mode is more desirable because it would minimize potential interference with rover mobility and would enable the antenna to be bistatically configured to eliminate early time range loss related to the T/R switch.

3.5. GPR Operation on Mars

[27] Preferred operation of the rover-deployable Mars GPR involves continuous data collection while roving at top speeds of up to 6 cm/sec (or about 50 m/hr). The possibility that antenna deployment might create a hazard to rover movement or navigation, however, requires that other deployment options also be considered. Ongoing consideration of a range of possible deployment systems precludes accurate estimation of time needed to extend and retract the antenna. Once deployed, however, data acquisition (includ-
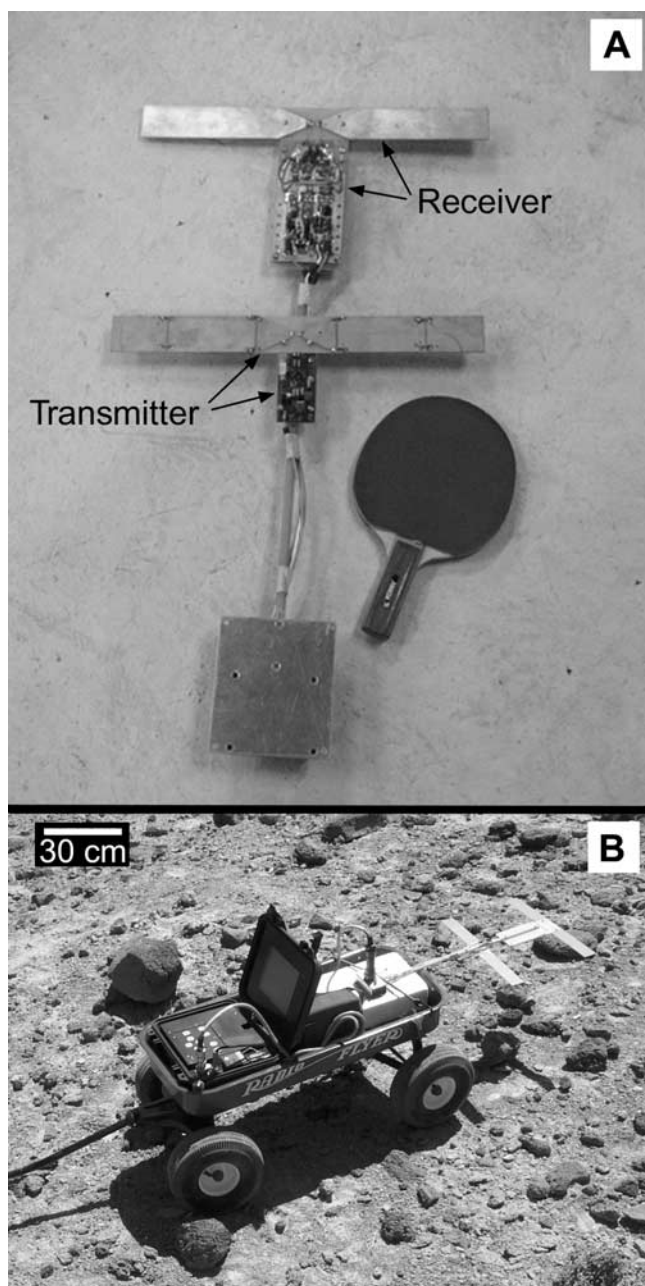
Figure 3. (a) Breadboard version of the high-frequency bistatic antenna being designed for the rover-deployable GPR, with a ping-pong paddle for scale. (b) Current deployed configuration during field tests used a metal wagon as a proxy for the rover. The breadboard operates at a central frequency of 600 MHz that can be easily modified by changing the width of the antenna fans. Design incorporates standard commercial connections to facilitate testing and does not incorporate a probable folding, retractable mechanism that would facilitate eventual above ground deployment and retraction from the rover body.

ing warm-up) requires less than two seconds. Deployment and collection of GPR data every ∼50−100 cm along a traverse during scheduled navigational and hazard-detection pauses would enable repeated, short-term deployment with minimal risk to rover mobility.

[28] Review of generic operation plans for the 2003 MER Rovers [*Crisp*, 2001] confirms that navigation and hazard detection pauses would frequently be accompanied by stereo imaging to assist in rover positioning. Coincident GPR deployment during these pauses would enable data collection along a series of closely spaced, precisely located stations. Because rover movement during early operations on the Martian surface would likely be confined to the immediate vicinity of the landing [*Crisp*, 2001], sufficient data could be collected to permit three-dimensional modeling of the shallow subsurface.

[29] A critical aspect of instrument design involves the ability to collect meaningful data within the limits imposed by downlink capabilities from Mars. One of the attractive characteristics of our GPR is a relatively low data rate and volume even during simultaneous operation of both antennas. For example, simultaneous operation at a range of up to 1000 ns along a rover transect covering 50 m in a day yields an estimated uncompressed data volume of only ∼0.3 Mb/d (Table 3). While this example includes assumptions regarding typical rover and GPR operations (Table 3), it nonetheless serves as a first-order proxy for probable data requirements imposed by operation of the instrument. For a situation where a higher sampling density or detection to greater depths is desirable, data stacking can be used to improve signal-to-noise and could be employed along sections of the rover traverse.

4. Field Tests in Mars Analog Environments

[30] Field-testing comprises an important step in evaluating the potential value of a rover-deployable GPR for constraining geologic setting and providing context for rover science instruments. In recognition of this, GPR data were collected during summer, 2001, at the site of the "blind" FIDO rover trials near the Cronese dry lakebed in southern California (Figure 6). More specifically, GPR data were collected adjacent to and across an actively aggrading wash bounded by Mesozoic dacitic rocks of the Soda Mountain Formation [*Grose*, 1959; *Walker and Wardlaw*, 1989]. Fresh bedrock is variably iron-rich and is overlain by a weathering zone, a variable thickness of eolian silt, and is capped by a cobbly stone pavement. Eolian silt and sand transported from topographically lower surfaces, and carried into the wash by runoff, dominate the alluvium. Cobbly longitudinal bars formed by locally transported dacitic fragments punctuate the sandy wash surface. GPR data were collected using a metal wagon as a proxy for the FIDO rover and a commercial GPR control unit was configured using a 400 MHz transducer. The longer wavelength commercial system incorporates the same basic electronics as those in the 600 MHz breadboard antenna, but enabled greater penetration.

[31] Conditions at the time of the field tests were less than optimal for radar investigations, as soils and alluvium adjacent to and in the wash had been variably moistened by recent rainfall. Resultant increases in substrate conductivity led to greatly reduced radar penetration depths. Nevertheless, excavation confirms that the GPR data define radar reflectors to depths of several meters, and that interpretation of the reflections constrains key aspects of the geologic setting.
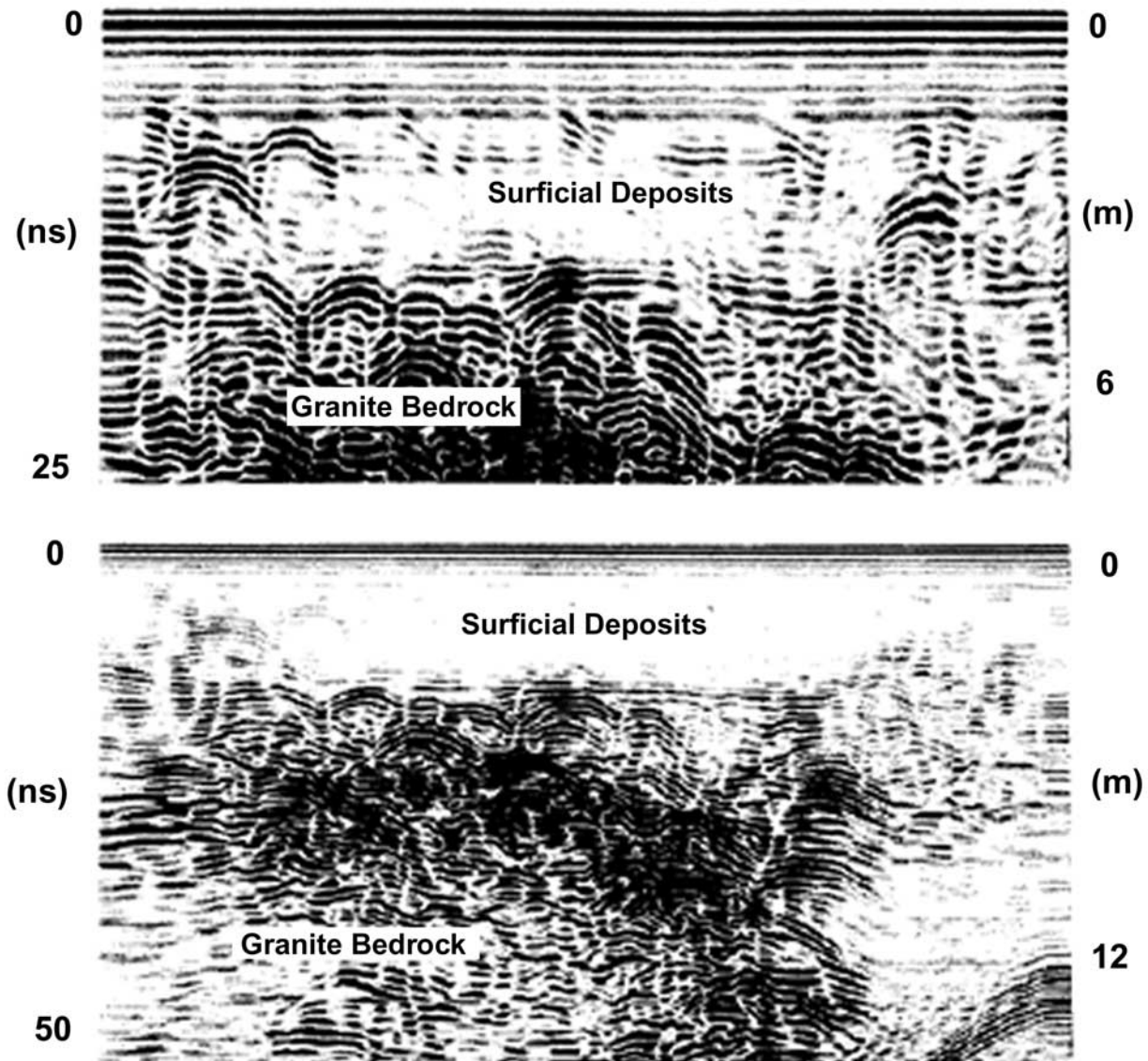
Figure 4. Sample data from the breadboard high-frequency bistatic antenna that was collected at the GSSI test bed facility in North Salem, NH. All data were collected along the same transect using pulse travel time ranges of 25 ns (top) and 50 ns (bottom) with the 600 MHz breadboard antenna shown in Figure 3. The antenna was deployed 15 cm above the ground and 30 cm from a metal box that served as a rover proxy. The antenna demonstrates the ability to distinguish sediments forming the test bed versus underlying surficial deposits (glacial in origin) versus fractured granitic bedrock to depths exceeding 10 meters. Construction involved use of standard GSSI parts: sampler board (1 GHz bandwidth) and pulse generator (70 V on a 50 ohm-load with a risetime of 700 pico seconds). Transect is approximately 10 meters in length.

[32] Data collected along transects from pavement and underlying silt-mantled bedrock surfaces down onto the wash (Figures 7a, 7b, and 7c) permit relationships between deposits and bedrock to be established. For example, data from pavement-mantled transects confirm that the cobbly surfaces mask a variably thick cobble-free horizon of eolian silt rather than in situ bedrock (Figures 7c, 8a, and 8b). Moreover, variations in the intensity of the reflection created by the eolian silt-to-bedrock and alluvium-to-bedrock interfaces provide a proxy for estimating the degree of weathering affecting the bedrock (Figure 8a) and defining relationships between bedrock and alluvium (Figure 8b). Bright bedrock reflections adjacent to cut-bank portions of the wash contrast with those beneath the eolian silt, do not correlate with a zone of enhanced moisture, and highlight the more abrupt and fresh interface created by alluvial stripping. GPR data reveal the alluvium is generally only ~1−2 m thick and that cobbles are mostly concentrated in the bar-forms noted above. Data from a location farther downstream (Figure 7b) indicate weathered bedrock extends laterally into
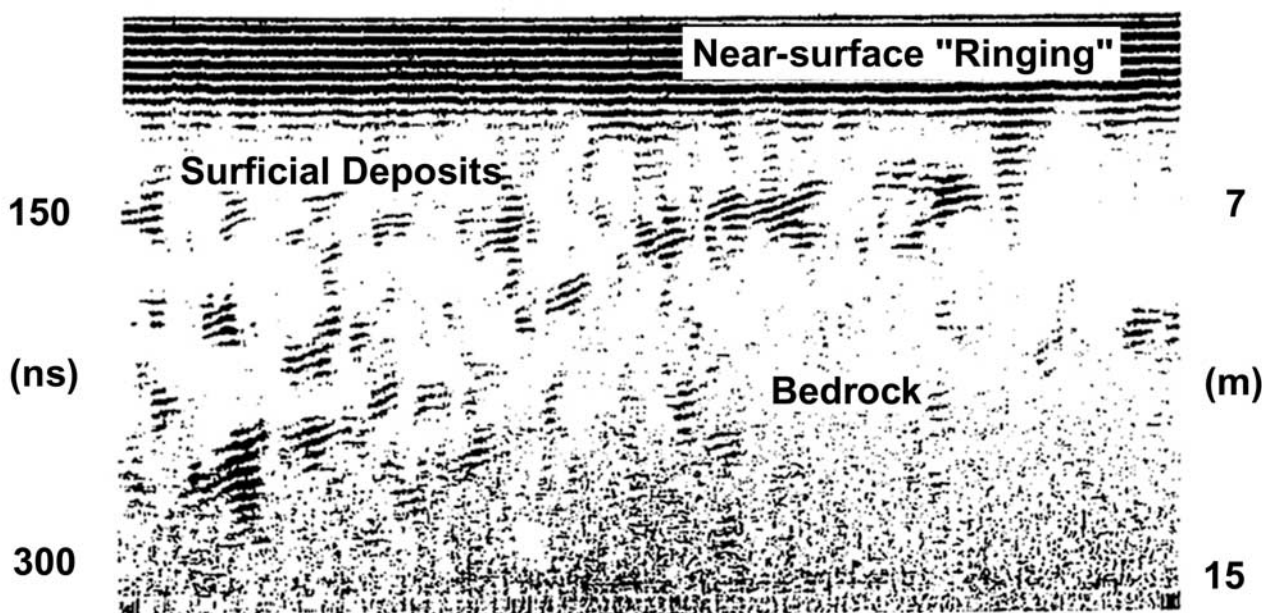
Figure 5. Sample data from the breadboard low-frequency "rat-tail" antenna that distinguishes reflections corresponding to a dipping surficial deposit-to-bedrock transition at 7 m and penetrates to overall depths of up to 15 m. Initial testing required use of bistatically configured, 40 cm long, resistivity loaded monopoles as antennas (central frequency 100 MHz). It is expected that data from the high-frequency antenna will provide coverage in the near surface "blind" zone caused by "ringing" in the top ~20 ns of the transect. Transect is approximately 10 meters in length.

the wash beneath a thin veneer of alluvium (Figure 8b) as a result of aggradation within the simultaneously laterally eroding wash.

[33] These results highlight how future interpretation of geologic setting on Mars might be in error, and how samples/measurements may be mis-targeted, without knowledge of shallow stratigraphy. Without GPR data, origin of the cobble-mantled surfaces at the FIDO site might be attributed to in situ weathering of bedrock or a nearby impact event rather than eolian deposition and lifting of the clasts via stone pavement formation [*McFadden et al.*, 1987; *Wells et al.*, 1987]. Similarly, GPR data can help target locations where a minimal thickness of stone pavement and silt maximizes ease of access to bedrock, or where sampling of alluvium may not be clouded by accidentally penetrating underlying bedrock.

5. Summary and Conclusions

[34] Based on the proven utility of GPR on the Earth and the potential to use GPR to resolve a number of questions related to the geologic setting at future Martian landing sites, the design and construction of an impulse GPR for possible rover-deployment on Mars in 2009 is well underway. The GPR has target mass, power, volume, and data volume limits of 0.5 kg, 3 W (peak), 3400 cc, and 0.3 Mb/d,

Table 3. Preliminary Estimate of GPR Data Requirements[a]

Antenna	Range, ns	Samples/scan	Scans/meter	Samples/meter	Bytes/meter
400	15	64	25	1600	
400	30	128	5	640	
400	60	256	1	256	
100	240	256	1	256	
			TOTAL	2752	5504

	Bytes/meter	Meters/day	Kilobytes/day
Raw data	5504	50	275
Modest compression	2752	50	138
High compression	550	50	28

[a]Estimated data/meter based on assumption of 10 samples per cycle to avoid oversampling. High-frequency antenna at 400 MHz is 2.5 nanoseconds per pulse. Range of 15 ns gives 6 cycles per scan, requiring 64 samples per scan. A 30 ns range would require 128 points per scan, and 60 ns would require 256. Because horizontal resolution decreases with penetration, and for highest possible data rate (data taken continuously while roving), taking near-surface data every 4 cm at 15 ns might yield 1 m penetration. Data might also be taken at a 30 ns range every 20 cm and at 60 ns every 100 cm. Low-frequency antenna is about 100 ns per cycle. Estimates are for uncompressed data.
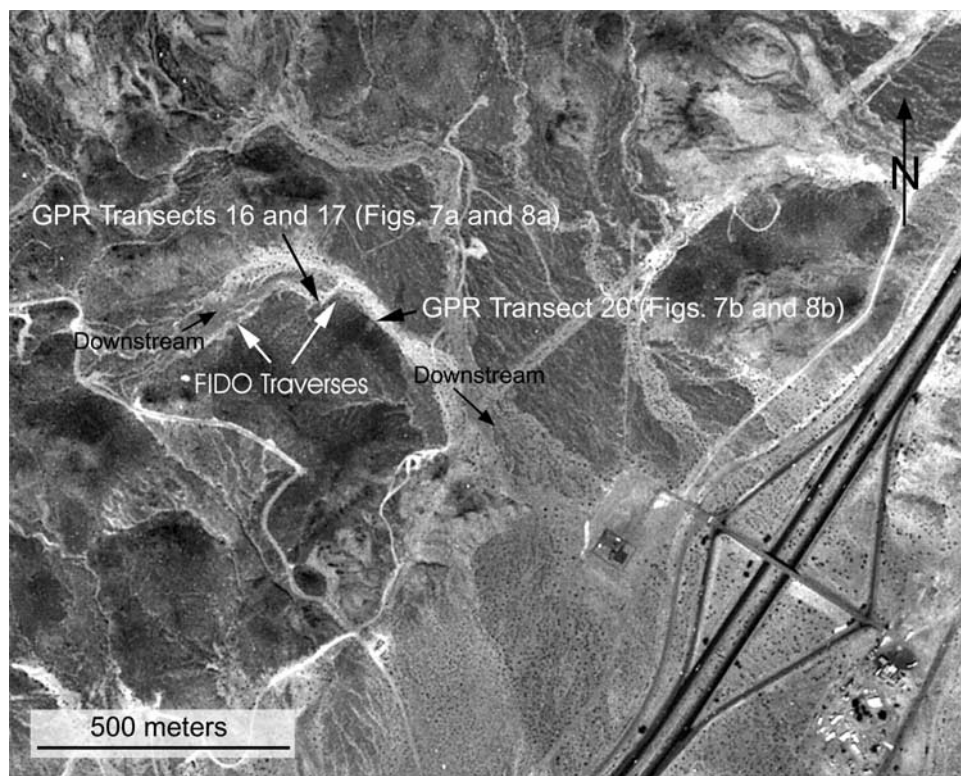
Figure 6. Air photograph of FIDO field test site near Cronese dry lakebed and approximately 16 kilometers west of Baker, California. Arrows denote locations along the wash where GPR data were collected in late July, 2001, in support of the rover trials and shown in Figures 7a and 7b and Figures 8a and 8b. Interstate highway 15 traverses the lower right corner of the photo for scale.

and will possess easily modified bistatic high-frequency (e.g., 500–600 MHz) and lower-frequency monostatic "rattail" (e.g., 100 MHz) antennas. The GPR should be capable of directly measuring in situ radar properties on Mars to depths of up to 10–20 m, thereby helping to constrain near-surface geology and structure.

[35] Initial testing with a GPR at the site of the 2001 FIDO rover field trials near Cronese dry lakebed, California, confirms the value of the instrument in defining radar reflections attributable to interfaces between surficial deposits (including eolian silt and alluvium) and underlying bedrock. These data permit first-order assignment of the processes responsible for shaping the present surface and for mapping the distribution of local depositional environments.

[36] As is the case for most remote sensing instruments, a rover-deployed GPR on Mars may not detect water unambiguously. Nevertheless, any local, near-surface occurrence of liquid water will lead to large, easily detected dielectric contrasts. Moreover, definition of stratigraphy and setting will help in evaluating the history of aqueous activity and where any water might occur and be accessible. Most importantly, perhaps, GPR can provide critical context for other rover and orbital data sets. Rover deployment of a GPR should enable three-dimensional mapping of local stratigraphy and could guide subsurface sampling. Although a number of environmental issues and tests will need to be completed before the GPR can be declared "flight-ready", such tests are common to all instruments and should be no more difficult to overcome than for other previously deployed systems.

References

Acuna, M. H., et al., Global distribution of crustal magnetization discovered by the Mars Global Surveyor MAG/ER Experiment, *Science*, *284*, 790–793, 1999.

Arvidson, R. E., R. Greeley, M. C. Malin, R. S. Saunders, N. Izenberg, J. J. Plaut, E. R. Stofan, and M. K. Shepard, Surface modification of Venus as inferred from Magellan observations of plains, *J. Geophys. Res.*, *97*, 13,303–13,317, 1992.

Banin, A., B. C. Clark, and H. Wanke, Surface chemistry and mineralogy, in *Mars*, edited by H. H. Kieffer, et al., pp. 1054–1089, Univ. of Ariz. Press, Tucson, 1992.

Barbin, Y., F. Nicollin, W. Kofman, V. Zolotarev, and V. Glotov, Mars 96 GPR program, *J. Appl. Geophys.*, *33*, 27–37, 1995.

Beaty, D. W., T. G. Farr, P. Gogineni, J. Grant, B. Grimm, C. Leuschen, G. R. Olhoeft, and A. Safaeinili, Report of the Virtual Instrument Science Definition Team on Surface EM Experiments for Mars 2007, JPL White Paper produced for NASA Headquarters, NASA, Washington, D. C., 2001.

Biccari, D., G. Picardi, R. Seu, A. Coradini, and R. Orosei, The Mars High Resolution Advanced Radar for 2005 space mission, in *Abstracts From the Conference on the Geophysical Detection of Subsurface Water on Mars*, edited by S. Clifford, J. George, and C. Stoker, pp. 9–10, *LPI Contrib. 1095*, Lunar and Planet. Inst., Houston, Tex., 2001.

Blaney, D. L., and T. B. McCord, Implications of the low carbonate abundance in the optical surface of Mars (abstract), *Proc. Lunar Planet Sci. Conf. 18th*, 97–98, 1990.
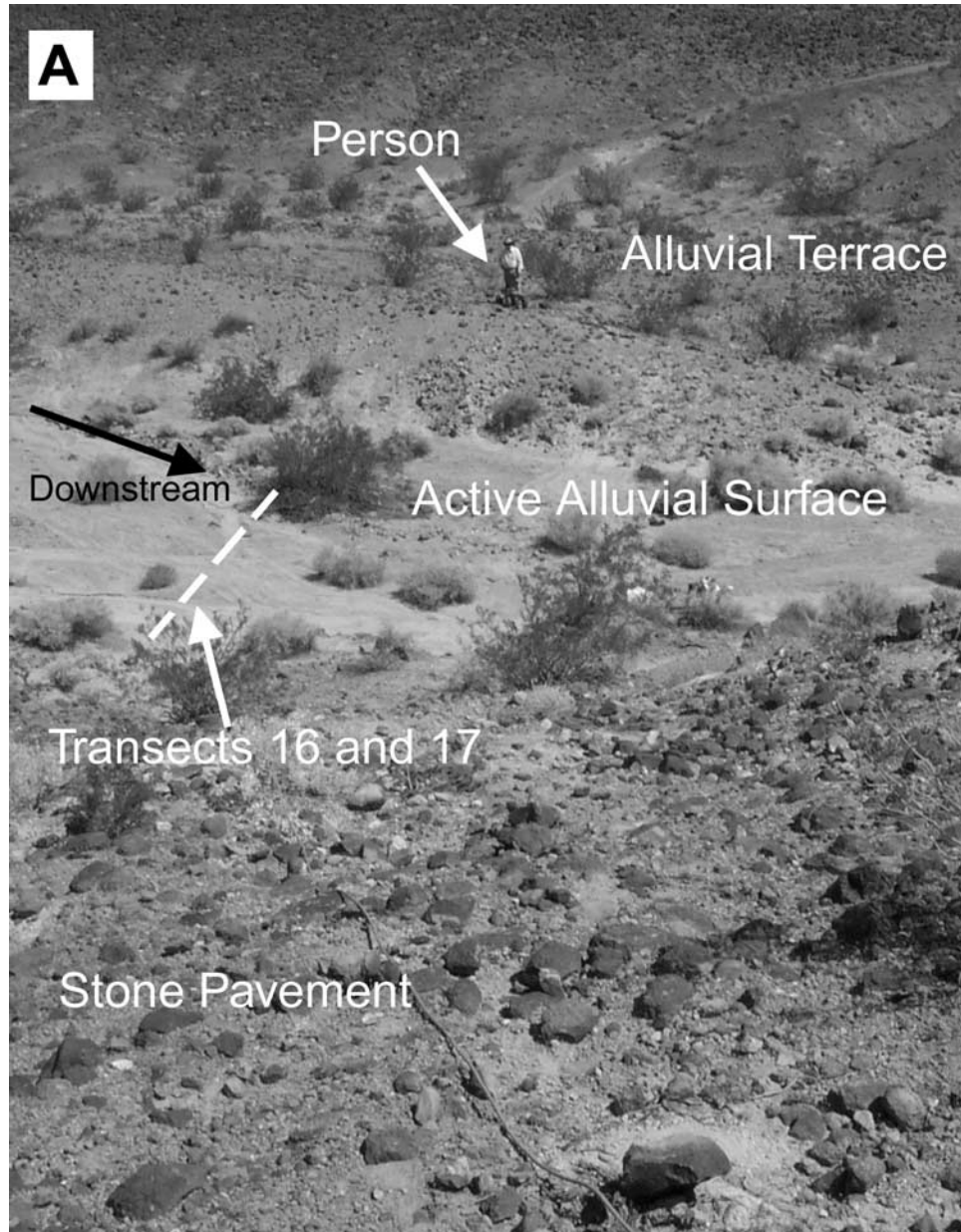
Figure 7. (a) View from SW to NE across stone pavement surface and wash crossed with GPR along transects 16 and 17 and shown in Figure 8a. The white dashed line marks the location of the transects (from lower left to upper right). (b) View to west from surface of wash and up along stone pavement surface. The location of transect 20 in Figure 8b is marked by white dashed line (from the pavement out onto the wash). Location is approximately 75 m downstream of (a) and westward lateral erosion of the wash has exposed weathered dacitic bedrock from beneath eolian silts and the pavement. Simultaneous aggradation of the wash then causes this bedrock surface to be only thinly buried beneath a cover of ~10–20 alluvium out to the area marked by the dashed line. (c) View of shallow pit excavated in the far foreground of (a) along transects 16 and 17 and confirming the occurrence of a silty, clast-free horizon beneath the pavement cobbles and above the weathered bedrock surface. The silty horizon is locally up to ~1 meter thick.
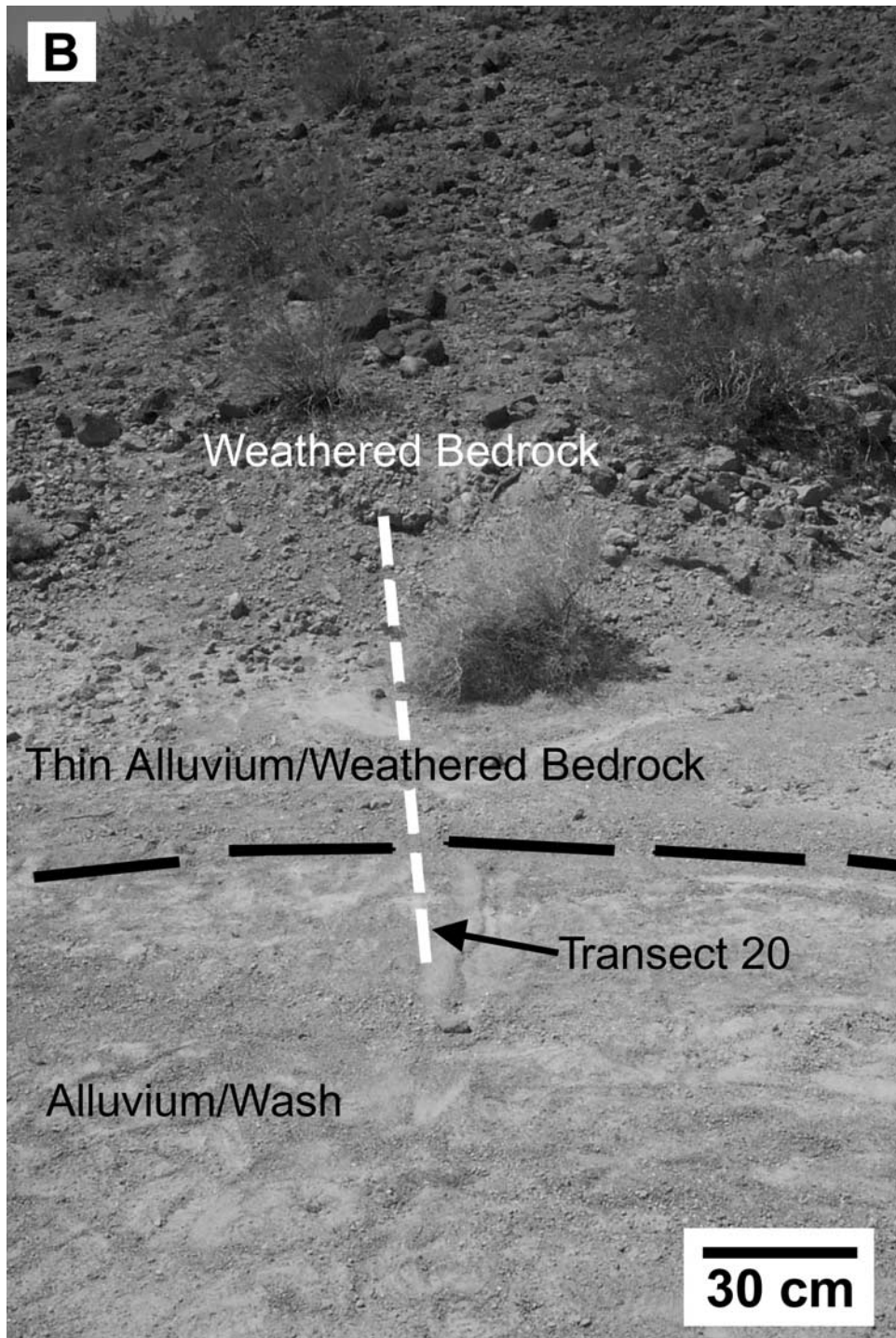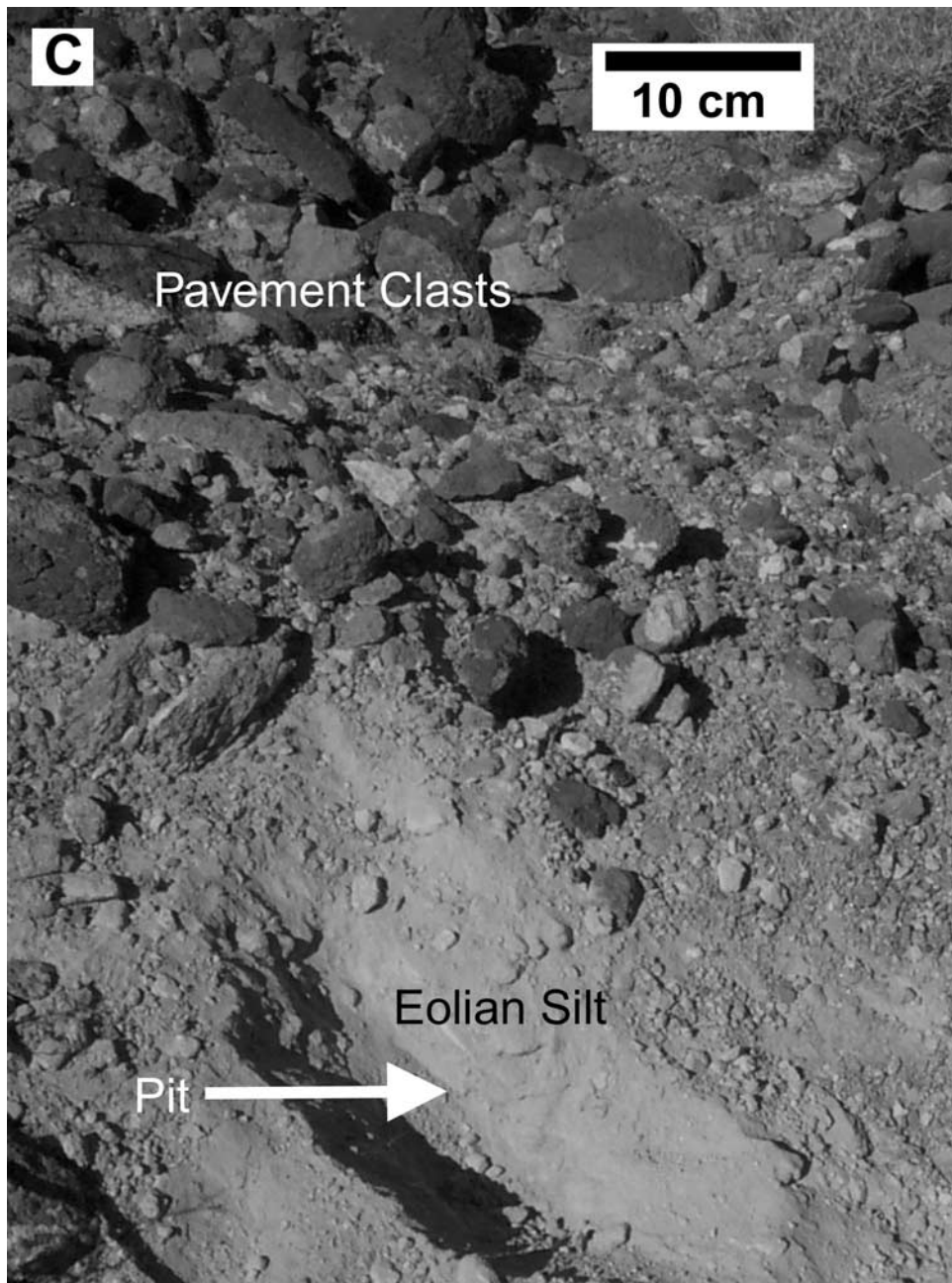
Figure 7.   (continued)
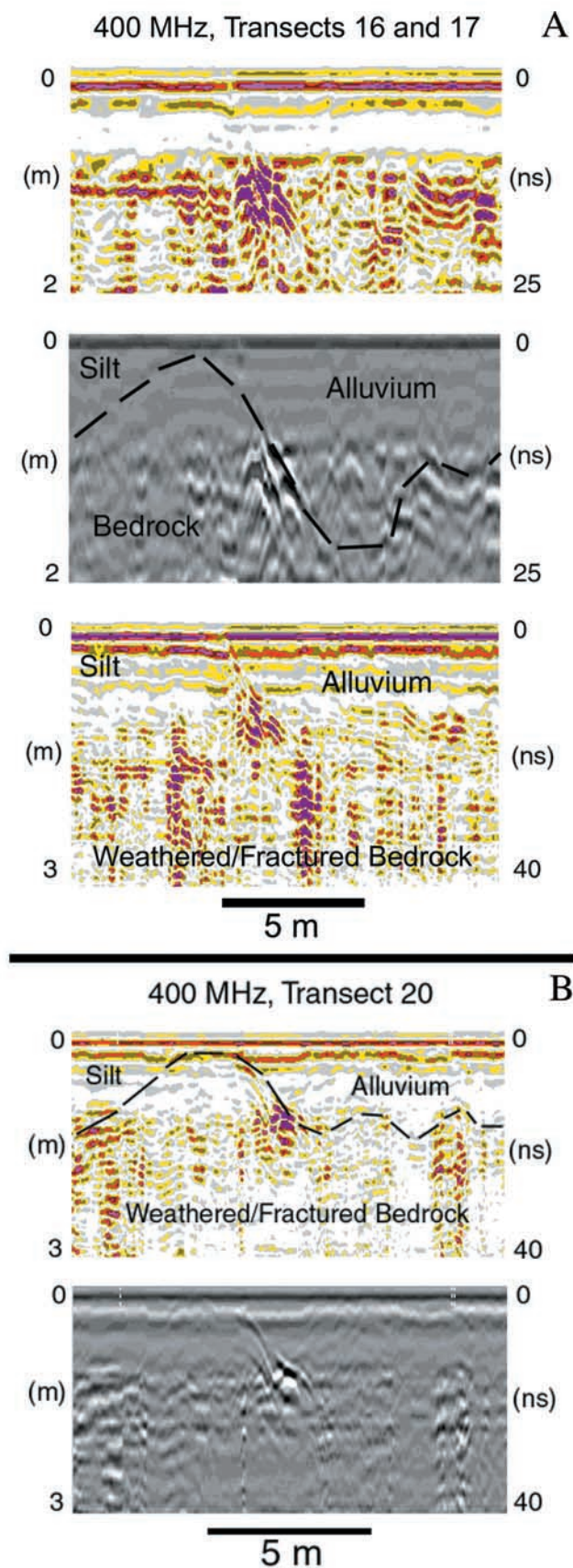
Figure 7.   (continued)

Figure 8. (opposite) Sample GPR data collected along transects shown in Figures 7a and 7b. In (a), the top two panels and the lower panel are from separate transects 16 and 17, respectively. The top two panels are the same data displayed in formats that highlight differing aspects of the data. These transects were completed from southwest-to-northeast along the same line shown in Figure 7a, but using differing time range/depth settings and confirm the repeatability of the GPR data. Pavement and underlying silt on the left portion of the transects pinches out along the margin of the aggrading wash where a brightening of the contact with the bedrock marks where erosion along the aggrading cut bank exposed a fresh surface that has then been buried. Alluvium is generally 1–2 meters thick with only a few cobbles (local parabolic reflections) beyond the limits of longitudinal bars. Much the same situation exists in (b) where both panels show differing displays of the same data collected along a single west-to-east transect 20. The location of the transect is shown in Figure 7b and crosses from the pavement-mantled bedrock out onto the aggrading alluvial surface. The data confirm the variably thin nature of the alluvium and reveal that bedrock extends well out into the wash where it is only thinly buried by alluvium. All data were collected using a 400 MHz transducer connected to a commercial GSSI GPR.

Butler, B. J., Martian "Stealth(s)" (abstract), *Proc. Lunar Planet Sci. Conf. 26th*, 199–200, 1995.

Butler, B. J., D. O. Muhlman, and M. A. Slade, Mercury: Full-disk radar images and the detection and stability of ice at the North Pole, *J. Geophys. Res.*, *98*, 15,003–15,024, 1993.

Campbell, B. A., and M. K. Shepard, Lava flow surface roughness and depolarized radar scattering, *J. Geophys. Res.*, *101*, 18,941–18,951, 1996.

Campbell, B. A., R. E. Arvidson, and M. K. Shepard, Radar polarization properties of volcanic and playa surfaces: Applications to terrestrial remote sensing and Venus data interpretation, *J. Geophys. Res.*, *98*, 17,099–17,113, 1993.

Campbell, B. A., B. R. Hawke, and T. W. Thompson, Regolith composition and structure in the lunar maria: Results of long-wavelength radar studies, *J. Geophys. Res.*, *102*, 19,307–19,320, 1997.

Campbell, B. A., D. B. Campbell, J. A. Grant, S. Hensley, T. A. Maxwell, J. J. Plaut, P. Rosen, M. K. Shepard, and R. Simpson, Orbital imaging radar and the search for water on Mars, in *Abstracts From the Conference on the Geophysical Detection of Subsurface Water on Mars*, edited by S. Clifford, J. George, and C. Stoker, pp. 16–17, *LPI Contrib. 1095*, Lunar and Planet. Inst., Houston, Tex., 2001.

Christensen, P. R., Regional dust deposits on Mars: Physical properties, age, and history, *J. Geophys. Res.*, *91*, 3533–3545, 1986.

Clifford, S., J. George, and C. Stoker, (Eds.), *Abstracts From the Conference on the Geophysical Detection of Subsurface Water on Mars*, *LPI Contrib. 1095*, Lunar and Planet. Inst., Houston, Tex., 2001.

Collins, M. E., and J. L. Kurtz, Assessing GPR performance in three soil geographic regions, paper presented at GPR'98: Seventh International Conference on Ground Penetrating Radar, Univ. of Kans., Lawrence, 1998.

Crisp, J., Proposal information package for the Mars Exploration Rover Mission Participating Science Program, NASA Announcement of Opportunity, Off. of Space Sci., NASA Headquarters, Washington, D. C., 2001.

Dyce, R. B., G. H. Pettengill, and A. D. Sanchez, Radar observations of Mars and Jupiter at 70 cm, *Astron. J.*, *72*, 771–777, 1967.

Elachi, C., Abstracts of the second space-borne imaging radar symposium, *JPL Publ. 86-26*, 233 pp., Jet Propul. Lab., Pasadena, Calif., 1986.

Evans, D. L., T. G. Farr, J. P. Ford, T. W. Thompson, and C. L. Werner, Multipolarization radar images for geologic mapping and vegetation discrimination, *IEEE Geosci. Remote Sens.*, *GE-24*, 246–257, 1986.

Fanale, F. P., J. R. Salvail, W. B. Banerdt, and R. S. Saunders, Mars: The regolith-atmosphere-cap system and climate changes, *Icarus*, *50*, 381–407, 1982.

Gaddis, L. R., Lava flow characterization at the Pisgah volcanic field, California, with multiparameter imaging radar, *Geol. Soc. Am. Bull.*, *104*, 703–965, 1992.

Goldspiel, J. M., and S. W. Squyres, Ancient aqueous sedimentation on Mars, *Icarus*, *89*, 392–410, 1991.

Goldspiel, J. M., S. W. Squyres, and D. G. Jankowski, Topography of small Martian valleys, *Icarus*, *105*, 479–500, 1993.

Goldstein, R. M., and W. F. Gillmore, Radar observations of Mars, *Science*, *141*, 1171–1172, 1963.

Golombek, M. P., et al., Overview of the Mars Pathfinder mission and assessment of landing site predictions, *Science*, *278*, 1743–1748, 1997.

Grant, J. A., Valley formation in Margaritifer Sinus, Mars, by precipitation-recharged ground-water sapping, *Geology*, *28*, 223–226, 2000.

Grant, J. A., and P. H. Schultz, Ground penetrating radar as a tool for investigation of near-surface stratigraphy on Mars (abstract), in *Martian Surface and Atmosphere Through Time: Workshop on Innovative Instrumentation for the In Situ Study of Atmosphere-Surface Interactions on Mars*, *LPI Tech. Rep. 92-07*, pp. 5–7, Lunar and Planet. Inst., Houston, Tex., 1992.

Grant, J. A., and A. Schutz, Development of a planetary ground penetrating radar (abstract), in *Deep Water Sounding on Mars Workshop*, NASA Ames Res. Cent., Mountain View, Calif., 1998.

Grant, J. A., P. H. Schultz, and W. K. Collins, Effectiveness of ground penetrating radar in Argentine loess: Implications for future Mars surface radar sounders (abstract), *Proc. Lunar Planet. Sci. Conf. 26th*, 497–498, 1995a.

Grant, J. A., P. H. Schultz, and J. O. Campos-Enriquez, Definition of shallow subsurface structure around the Chicxulub impact crater using ground penetrating radar (abstract), *Proc. Lunar Planet. Sci. Conf. 26th*, 495–496, 1995b.

Grant, J. A., C. Koeberl, W. U. Reimold, P. H. Schultz, and D. Brandt, Degradation history of the Roter Kamm impact crater, Namibia, *J. Geophys. Res.*, *102*, 16,327–16,388, 1997.

Grant, J. A., M. J. Brooks, and B. E. Taylor, New constraints on the evolution of Carolina Bays from ground penetrating radar, *Geomorphology*, *22*, 325–345, 1998.

Grant, J. A., B. A. Campbell, and A. E. Schutz, A rover deployed ground penetrating radar on Mars, in *Abstracts From the Conference on the*

Geophysical Detection of Subsurface Water on Mars, edited by S. Clifford, J. George, and C. Stoker, pp. 41–42, LPI Contrib. 1095, Lunar and Planet. Inst., Houston, Tex., 2001.

Greeley, R., and J. E. Guest, Geologic map of the eastern equatorial region of Mars, *U.S. Geol. Surv. Map I-1802-B*, 1987.

Grose, L. T., Structure and petrology of the northeast part of the Soda Mountains, San Bernardino County, California, *Geol. Soc. Am. Bull.*, *70*, 1509–1583, 1959.

Harmon, J. K., R. E. Arvidson, E. A. Guinness, B. A. Campbell, and M. A. Slade, Mars mapping with delay-Doppler radar, *J. Geophys. Res.*, *104*, 14,065–14,089, 1999.

Head, J. W., H. Hiesinger, M. A. Ivanov, M. A. Kreslavsky, S. Pratt, and B. J. Thomson, Possible ancient oceans on Mars: Evidence from Mars Orbiter Laser Altimeter data, *Science*, *286*, 2134–2137, 1999.

Heggy, E., P. Paillou, G. Ruffie, J. Malezieux, F. Costard, and G. Grandjean, On sounding radar performances for Martian subsurface water detection, in *Abstracts From the Conference on the Geophysical Detection of Subsurface Water on Mars*, edited by S. Clifford, J. George, and C. Stoker, pp. 47–48, *LPI Contrib. 1095*, Lunar and Planet. Inst., Houston, Tex., 2001.

Institute for Space Research, *Mars-94, Unmanned Spacecraft Mission to Mars*, 55 pp., Russ. Acad. of Sci., Moscow, Russia, 1992.

Leuschen, C. J., S. P. Gogineni, S. M. Clifford, and R. K. Raney, Design of a ground-penetrating radar for Mars, in *Abstracts From the Conference on the Geophysical Detection of Subsurface Water on Mars*, edited by S. Clifford, J. George, and C. Stoker, pp. 64–65, *LPI Contrib. 1095*, Lunar and Planet. Inst., Houston, Tex., 2001.

Malin, M. C., and K. S. Edgett, Sedimentary rocks of early Mars, *Science*, *290*, 1927–1937, 2000.

Malin, M. C., and K. S. Edgett, The Mars Global Surveyor Mars Orbiter Camera: Interplanetary Cruise through Primary Mission, *J. Geophys. Res.*, *106*, 23,429–23,571, 2001.

Malin, M. C., et al., Early views of the Martian surface from the Mars Orbiter Camera of Mars Global Surveyor, *Science*, *279*, 1681–1685, 1998.

McFadden, L. D., S. G. Wells, and M. J. Jercinovich, Influences of eolian and pedogenic processes on the origin and evolution of desert pavements, *Geology*, *15*, 504–508, 1987.

McKay, D. S., E. K. Gibson Jr., K. L. Thomas-Keprta, H. Vali, C. S. Romanek, S. J. Clemett, X. D. F. Chillier, C. R. Maechling, and R. N. Zare, Search for past life on Mars: Possible relic biogenic activity in Martian meteorite ALH84001, *Science*, *273*, 924–930, 1996.

Muhleman, D. O., Radar observations of Mars, Mercury, and Titan, *Annu. Rev. Earth Planet. Sci.*, *23*, 337–374, 1995.

Muhleman, D. O., B. J. Butler, A. W. Grossman, and M. A. Slade, Radar images of Mars, *Science*, *253*, 1508–1513, 1991.

Olhoeft, G. R., Selected bibliography on ground penetrating radar, paper presented at Symposium on Applications of Geophysics in Engineering and Environmental Problems, pp. 463–520, Colo. School of Mines, Golden, 1988.

Olhoeft, G. R., Ground penetrating radar on Mars, paper presented at GPR '98: 7th International Conference on Ground Penetrating Radar, pp. 387–392, Univ. of Kans., Lawrence, 1998a.

Olhoeft, G. R., Electrical, magnetic, and geometric properties that determine ground penetrating radar performance, paper presented at GPR '98, 7th International Conference on Ground Penetrating Radar, pp. 177–182, Univ. of Kans., Lawrence, 1998b.

Olhoeft, G. R., and D. W. Strangeway, Dielectric properties of the first 100 meters of the Moon, *Earth Planet. Sci. Lett.*, *24*, 394–404, 1974.

Ori, G. G., and F. Ogliani, Potentiality of ground penetrating radar for the analysis of the stratigraphy and sedimentology of Mars, *Planet. Space Sci.*, *44*, 1303–1315, 1996.

Paige, D. A., The Mars Polar Pathfinder (abstract), in *Mars Surveyor-Science Objectives/Measurement Requirements Workshop*, pp. 126–127, Jet Propul. Lab., 1994.

Parker, T. J., R. S. Saunders, and D. M. Schneeberger, Transitional morphology in west Deuteronilus Mensae, Mars: Implications for modification of the lowland/upland boundary, *Icarus*, *82*, 111–145, 1989.

Peeples, W. J., W. R. Sill, T. W. May, S. H. Ward, R. J. Phillips, R. L. Jordan, E. A. Abbott, and T. J. Killpack, Orbital radar evidence for lunar subsurface layering in Maria Serentitatis and Crisium, *J. Geophys. Res.*, *83*, 3459–3468, 1978.

Phillips, R. J., et al., Apollo Lunar Sounder experiment, in *Apollo 17: Preliminary Science Report*, *NASA Spec. Publ.*, NASA SP-330, 22-1–22-26, 1973.

Planetary Surface Instrument Workshop, *NASA Tech Memo. 95-05*, Lunar and Planet. Inst., Houston, Tex., 1995.

Plaut, J. J., A ground penetrating radar experiment from orbit (abstract), in *Deep Water Sounding on Mars Workshop*, NASA Ames Res. Cent., Mountain View, Calif., 1998.

Reineix, A., B. Martinat, J. J. Berthelier, and R. Ney, FDTD method for the theoretical analysis of the Netlander GPR, in *Abstracts From the Conference on the Geophysical Detection of Subsurface Water on Mars*, edited by S. Clifford, J. George, and C. Stoker, pp. 88–89, *LPI Contrib. 1095*, Lunar and Planet. Inst., Houston, Tex., 2001.

Rieder, R., T. Economou, H. Wanke, A. Turkevich, J. Crisp, J. Bruckner, G. Dreibus, and H. Y. McSween Jr., The chemical composition of Martian soil and rocks returned by the mobile alpha proton X-ray spectrometer: Preliminary results from the X-ray mode, *Science, 278*, 1771–1774, 1997.

Schaber, G. G., J. F. McCauley, C. S. Breed, and G. R. Olhoeft, Shuttle Imaging Radar: Physical controls on signal penetration and subsurface scattering in the eastern Sahara, *IEEE Trans. Geosci. Remote Sens., 24*, 603–623, 1986.

Settle, M., Formation and deposition of volcanic sulfate aerosols on Mars, *J. Geophys. Res., 84*, 8343–8354, 1979.

Simpson, R. A., J. K. Harmon, S. H. Zisk, T. W. Thompson, and D. O. Muhleman, Radar determination of Mars surface properties, in *Mars*, edited by H. H. Kieffer, et al., pp. 652–685, Univ. of Ariz. Press, Tucson, 1992.

Thompson, T. W., J. B. Pollack, M. J. Campbell, and B. T. O'Leary, Radar maps of the Moon at 70-cm wavelength and their interpretation, *Radio Sci., 5*, 253–262, 1970.

Thomson, B. J., and J. W. Head, Utopia Basin, Mars: Characterization of topography and morphology and assessment of the origin and evolution of basin internal structure, *J. Geophys. Res., 106*, 23,209–23,230, 2001.

Toulmin, P., A. K. Baird, B. C. Clark, K. Keil, H. J. Rose, R. P. Christian, P. H. Evans, and W. C. Kelliher, Geochemical and mineralogical interpretations of the Viking inorganic chemical results, *J. Geophys. Res., 82*, 4625–4634, 1977.

Ulaby, F. T., T. Bengal, J. East, M. C. Dobson, J. Garvin, and D. Evans, Microwave dielectric spectrum of rocks, *Radiat. Lab., Rep. 23817-1-TU*, Univ. of Mich., Ann Arbor, 1988.

Ulriksen, C. P. F., Application of impulse radar to civil engineering, Ph.D. thesis, Univ. of Technol., Lund, Sweden, 1982.

Walker, J. D., and B. R. Wardlaw, Implications of Paleozoic and Mesozoic rocks in the Soda Mountains, northeastern Mojave Desert, California, for late Paleozoic and Mesozoic Cordilleran orogenesis, *Geol. Soc. Am. Bull., 101*, 1574–1583, 1989.

Wells, S. G., L. D. McFadden, and J. C. Dohrenwend, Influence of late Quaternary climate changes on geomorphic and pedogenic processes on a desert piedmont, Eastern Mojave Desert, California, *Quat. Res., 27*, 130–146, 1987.

Zent, A. P., F. P. Fanale, and L. E. Roth, Possible Martian brines: Radar observations and models, *J. Geophys. Res., 95*, 14,531–14,542, 1990.

————————————————

B. Campbell and J. Grant, Center for Earth and Planetary Studies, National Air and Space Museum, Smithsonian Institution, 4th Street and Independence Avenue SW, Washington, DC 20560-0315, USA. (GrantJ@nasm.si.edu)

A. E. Schutz, Geophysical Survey Systems, Inc., 13 Klein Drive, North Salem, NH 03073, USA.